Simulation of the flow strength and microstructure of titanium aluminide in hot forging

M. C. ABERNATHY
Louisiana State University, Mechanical Engineering Department, Baton Rouge, LA 70803, USA

R. A. MIRSHAM
Southern University, Mechanical Engineering Department, Baton Rouge, LA 70813, USA
E-mail: mirshams@unt.edu

A. RAMAN
Louisiana State University, Mechanical Engineering Department, Baton Rouge, LA 70803, USA

B. Q. LI
School of Materials and Mechanics, Washington State University, Pullman, WA, USA

A. A. WERESZCZAK
Oak Ridge National Laboratory, Oak Ridge, TN, USA

The main purpose of this investigation is to develop a mathematical relationship for the flow strength based on microstructure evolution during the hot forming of titanium aluminide. For engineering applications, gamma titanium-aluminide which is composed of 46–50 at.% Al is desired in a duplex grain microstructure. Thermomechanical processing of this alloy requires a temperature of 0.60–0.75 T_M (melting point) in order to properly control the microstructure and grain growth. Compression tests were conducted in the temperature range between 950–1100°C at strain rates of 0.001/s and 0.1/s to develop a duplex phase microstructure, gamma with 5–20% α_2. By using the experimental data, mathematical relationships were verified for different stages of hardening, recovery, recrystallization, and grain growth. The simulation was based on the theory used in the Sandstrom and Lagneborg model and the numerical analysis approach developed by Pietrzyk. The simulation proved that the model and numerical simulation well-presented the compression deformation of titanium-aluminide alloys at constant strain rates.
© 2001 Kluwer Academic Publishers

1. Introduction

Elevated temperature applications of two-phase (duplex) gamma titanium-aluminide have been investigated in recent years in the aeronautical, aerospace, and automotive industries to take advantage of the alloy's lightweight, high strength, and creep resistance at high temperatures. The major advantage is that the titanium-aluminide (Ti-Al) alloy has a high strength to weight ratio for an application at elevated to high temperatures. A major concern to these industries is the alloy's poor ductility at room temperature which necessitates thermomechanical processing at high temperatures, around 0.6–0.75 T_S (solidus temperature), to control the microstructure and obtain attractive properties for the industry [1, 2]. To improve the mechanical properties for application in high temperature, alloying elements have been added to the titanium-aluminide alloys: Nb, for increasing strength and oxidation resistance; Mn for increasing the ductility and oxidation resistance; and Mo for increasing strength, creep resistance, oxidation resistance, spalling resistance, and corrosion resistance. Further, other elements such as W are also included for oxidation resistance, spalling resistance, and reduction of grain size and Si is added for oxidation resistance and grain refinement.

It has been found that for optimum properties in engineering applications, the major constituent should be the intermetallic compound TiAl (gamma-γ) with minor amounts of the secondary phase Ti_3Al (α_2). Titanium aluminide alloys of engineering interest contain between 5 to 20 volume percent of the secondary phase α_2-Ti_3Al [3]. Ti-48Al has its best ductility with an optimum volume ratio 5–15% of α_2/γ, below which grain growth becomes pronounced and above which the brittle α_2 phase reduces the ductility effects of refinement in microstructure. Since gamma is the major,

dominant phase, the duplex-phase alloy also is called the gamma titanium aluminide. In the past twenty years, researchers have conducted experiments on the gamma titanium aluminide alloy to determine its mechanical properties [4, 5] and microstructural deformation during hot forging wherein dynamic recrystallization has a major role in the grain refinement and formation of more stable microstructure.

In the model by Sandstrom and Lagneborg [6, 7] and numerical simulation by Pietryzk [8], dynamic recrystallization and grain growth are derived for a single-phase alloy based on the dislocation density in the alloy. The current paper presents the effects of precipitates or secondary phases on the flow stress and integration of them in the above model for characterizing the deformation of titanium aluminide in hot forging.

2. Experimental procedure

Howmet Corporation in Whitehall, Michigan processed the γ-TiAl alloy of composition Ti-47Al-2Nb-1Mn-0.5Mo-0.5W-0.2Si by investment casting followed by Hot Isostatic Pressing (HIPing) and annealing. Precision Industries of Baton Rouge, Louisiana machined the cylindrical compression test specimens of the alloy with the following dimensions: height 8.89 ± 0.25 mm $(0.350 \pm 0.010$ inch) and diameter 6.35 ± 0.03 mm $(0.2.250 \pm 0.001$ inch). The top and bottom surfaces were beveled at $45°$ and the diameter got reduced slightly to 6.30 ± 0.03 mm $(0.248 \pm 0.001$ inch). The parallelness and perpendicularity of the circular cross sections with respect to cylinder axis were 0.002 inches. The compression tests were carried out using an Instron 1332, model 8500, at the High Temperature Material Laboratory (HTML), Oak Ridge National Laboratory (ORNL), Oak Ridge, Tennessee. Molybdenum foil (100–150 μm thick) was used as sandwich between the beveled specimen end surfaces and α-SiC rams. A 102-mm high pancake style controlled temperature furnace was used to heat the specimens to the desired temperature. Fig. 1 shows the compression test setup with extensometer. The tests ranged in time from 50–500 seconds depending on the test strain rate. The strain rates were derived from a compliance curve obtained after calibrating the instrument with known strain rate data based on LVDT readings. The thermal expansion was also taken into account and it was de-

termined to be the following: 0.124 mm for 950°C, 0.133 mm for 1000°C, and 0.151 mm for 1100°C. Thus, the actual strain rates used during the tests were found to be 0.107/s and 0.00107/s. Also, to prevent the damaging or shattering of the compression load train, load limits were set at 16 kN for 0.1/s and 20–24 kN for 0.001/s. The tests were designed for a compression of 50%, however, due to load limitations, the amount of compression obtained ranged from 2% to 59%. For metallographic examination, the specimens were cut to ASTM specifications and parallel to the cylindrical axes using a Buehler low speed diamond saw in the HTML. The specimens were polished with a vibration grinder and Buehler polisher, and etched using Krolling reagent (5 ml HF, 10 ml HN0$_3$, and 85 ml H$_2$O) [9]. The microstructural images were taken using a Hitachi S800 scanning electron microscope with a digital camera mounted on the microscope. The average grain size was then calculated based on magnification, image dimensions, and distribution.
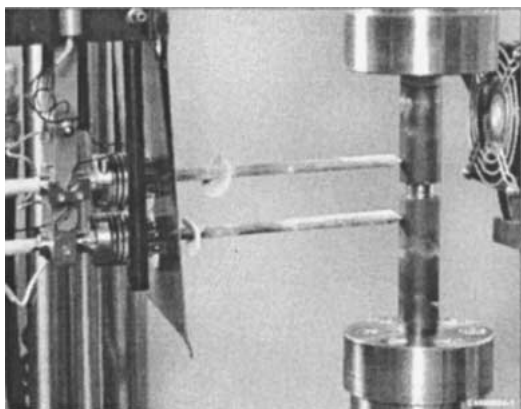
3. Results and discussion
3.1. Modeling fundamentals and simulation
During the hot forging process the mechanisms controlling the flow stress are hardening and recovery. The mechanical properties of the alloy during hot deformation vary as a result of a balance between the work hardening (strain hardening) and dynamic softening (dynamic recovery and dynamic recrystallization) processes [10]. These effects are illustrated using various microstructures and experimental-theoretical stress-strain curves. Sabinash, Sastry and Jerina [5] note that the dynamic recrystallized microstructure can display evidence of rapid flow softening due to recovery and dynamic recrystallization, or gradual strain hardening.

Dynamic recrystallization is characterized by operations at low temperatures/high strain rates or high temperatures/low strain rates. Dynamic recrystallization occurs after a distinct stress maximum on hot working stress-strain curves after which a steady-state stress, $\sigma_s < \sigma_{(max)}$, is eventually attained. Roberts and Ahlblom [11] stated that a critical deformation or strain, ε_c, is necessary in order to initiate dynamic recrystallization at a given temperature. Sandstrom and Lagneborg indicated that the behavior of the stress-strain curve depends critically on whether $\varepsilon_x < \varepsilon_c$ or $\varepsilon_x > \varepsilon_c$. In their research it was found that when $\varepsilon_x \ll \varepsilon_c$, one crystallization cycle is completed before another one starts, thus a periodic stress-strain curve results [6]. However, when $\varepsilon_x \gg \varepsilon_c$, one crystallization cycle is not completed before another one starts, thus interference occurs, resulting in a smooth stress-strain curve. Thus, the fact is established that dynamic recrystallization occurs in a straining element in stages and does depend on the strain rate. Significant research has evolved to demonstrate the experimental behavior of the duplex γ-TiAl alloy, Semiatin and Seetharaman [12–15], while Hoffman and Blum [16] developed a simple model of dynamic recrystallization of titanium-aluminide alloy. The basis for the flow behavior constitutive model is the assumption that the formation of dislocation populations determines the evolution of stress during

Figure 1 Compression test setup with extensometer.

plastic deformation. Work hardening is caused by the increase in the dislocation density and the recovery, and the softening occurs due to a drop in the dislocation density. Once the dislocation density is calculated, we can calculate the yield strength of the material by using the relation:

$$\sigma = \alpha \mu b \sqrt{\rho} \qquad (1)$$

where σ is true stress, α is a constant (0.5–1), μ is the shear modulus, b is the Burgers vector, and ρ is the average dislocation density. In our modeling effort, we take internal variable approach, as proposed by Sandstrom and Langeborg [6], to describe (a) The work hardening, (b) The dynamic recovery, (c) The dynamic recrystallization, and (d) The grain growth.

It is emphasized that the internal stresses are the key to understanding the plastic deformation behavior of γ-TiAl alloys. However, the components that determine whether dynamic recrystallization will occur can be defined from the following differential equation [8]

$$\frac{dG(\rho_d, t)}{dt} = \phi(\Delta\varepsilon) - g(\varepsilon) - \frac{v\gamma}{D} \cdot m \cdot \tau \cdot \rho_d \cdot G(\rho_d, t) \qquad (2)$$

where $G =$ dislocation population concentration, $\rho =$ dislocation density, $\phi(\Delta\varepsilon) =$ hardening for strain ε, $g(\varepsilon) =$ recovery, $v =$ grain boundary velocity, $\gamma =$ fraction of subgrain boundaries that are migrating, $D =$ grain size, $m =$ mobility of grain boundary, and $\tau =$ average energy per unit length of dislocation.

In order for movement of dislocations across grain boundaries to occur, a critical dislocation density must be obtained. The following is the equation for critical dislocation density, ρ_{cr}, derived by Roberts and Ahlblom [11]:

$$\rho_{cr} = \left(\frac{16 \cdot S \cdot \dot{\varepsilon}}{3 \cdot b \cdot l \cdot m \cdot \tau^2} \right)^{1/3} \qquad (3)$$

where $S =$ grain boundary energy, $m =$ mobility of the grain boundary; $l =$ cell size, $\tau =$ amount of energy required to cause movement of a dislocation. More detailed information are given in the Ref. [17].

To determine the final dislocation density, ρ_I, the following parameters must be calculated: ρ_ε, and ρ_{DRV}. The general calculation of the dislocation density after testing can be determined using the following equation:

$$\rho_I = (\rho_o + \rho_\varepsilon) - \rho_{DRX} \qquad (4)$$

where ρ_o, ρ_ε, ρ_{DRX} correspond to original, strain hardening and dynamic recrystallization dislocation density, respectively. In order for dynamic recrystallization to occur, $\rho_I \geq \rho_{cr}$.

Table I, using equations derived by Sandstrom and Lagneborg [6, 7] and Pietrzyk [6, 8], was used to illustrate the cycles for the simulation of a dynamic recrystallized alloy.

3.2. Validation of simulation
3.2.1. Microstructure evolution
In general, the internal state variable formulation of plastic deformation may be expressed in the following form

$$\frac{ds_n}{dt} = f_n(\varepsilon, \dot{\varepsilon}, T, s_1, \ldots, s_m) \qquad 1 < n < m$$

where s_i ($i = 1, \ldots, m$) is the mth internal variable, f_n the evolution equation for internal variable n and T the temperature. The internal variables can be scalars, vectors or tensors and they represent material microstructures such as dislocation density and grain size. The internal and external variables together describe the material behavior completely. The equations describing the material microstructure evolution (Table I) are a set of ordinary differential equations involving time as an independent variable. This set of equations is solved following the procedures as described by Pietrzyk [8, 18, 19].

In the numerical simulation of the model, initially, the whole spectrum of dislocation densities is divided into a number of equal intervals of size $\Delta\rho_0$. Therefore, according to the definition of

$$\sum_{i=1}^{n} G_i = 1$$

distribution function, the condition is always met during the simulation. In the above equation,

$$G_i = G(\rho_i, t)\Delta\rho_0$$

During the simulation, Grain size and recrystallized volume fraction are given for each interval and the

TABLE I Equations for the modeling and numerical simulation based on dislocation density [6, 18, 19]

Eqn. no.	Process	Variables	Condition	Sandstorm/Lagneborg equations: (a) mathematical model [6]	Pietrzyk equations: (b) Numerical simulation [19]
5	Hardening	$\Delta\rho, \rho$	$\varepsilon > 0$	$\dfrac{d\rho}{d\varepsilon} = \dfrac{1}{bl}$	$\Delta\rho_\varepsilon = \varepsilon^* \dfrac{\Delta t}{bl}$
6	Recovery	$\Delta\rho, \rho$	Always	$\dfrac{d\rho}{dt} = -2\tau\rho^2 M_o \exp\dfrac{-Qm}{RT}$	$\Delta\rho = -2^*\tau^*\rho^{2*}M^*\Delta t$
7	Recrystallization	G, X, ρ	$\rho > \rho_{cr}$	$\dfrac{dX}{dt} = \dfrac{v\gamma\tau^*}{D}G\rho m_o^* \exp\dfrac{-Qm}{RT}$	$\Delta X = \dfrac{v\gamma\tau^*}{D}G^*\rho^*m$
8	Grain refinement	D	$\rho > \rho_{cr}$	$\dfrac{dD}{dt} = -D^* \dfrac{dX^*}{dt} \ln N$	$\Delta D = -D^*\Delta X^* \ln N$
9	Grain growth	D	Always	$\dfrac{dD}{dt} = \sigma_g^* \dfrac{m_o^*}{D} \exp\dfrac{-Qm}{RT}$	$\Delta D = \dfrac{m\sigma_g}{D}(\Delta t)$

$l =$ path length, $M_o =$ initial mobility of recovery, $\tau =$ average energy per unit length of dislocation, $v =$ grain boundary velocity, $\gamma =$ fraction of subgrain boundaries which are migrating, $m_o =$ initial grain boundary mobility, $G =$ dislocation population concentration, $D =$ grain size, $X =$ dynamic recrystallization, $N =$ number of recrystallized grains per old grains, and $\sigma_g =$ stress acting on the grain.

level of the average dislocation density in the interval is prescribed. As a consequence, the arrays $D(n)$, $\Delta\rho(n)$ and $G(n)$ are introduced in the program. The deformation process is simulated by dividing the whole process into a number of time steps of size Δt. For each time step, five cycles (i.e., hardening, recovery, recrystallization, and grain refinement and grain growth) are considered. Here, the cycle means performing the process (e.g. hardening, recovery etc.) over the whole spectrum of dislocation densities once. The computational procedure described by Pietrzyk [19] was adopted in this numerical approach and further descriptions are given in Reference [20].

3.2.2. Experimental validation

γ-TiAl was characterized by a duplex microstructure consisting of TiAl and Ti_3Al, with the dynamic recrystallized stress-strain curves being characterized by a distinct peak at the beginning stages of the curve followed by a gradual smoothing until a flat line appears (flow softening). The simulated curves are based on the characteristics of the experimental curves. As shown in Fig. 2, the as-received microstructure of the titanium-aluminide alloy has a near-lamellar microstructure with equiaxed grains along the boundaries. The material has high strength with some ductility.

In the compression test conducted at 950°C with 0.001/s strain, the lamellar grains have been transformed into finer grains containing both γ and α_2 phases, as shown in Fig. 3. The reduction in grain size
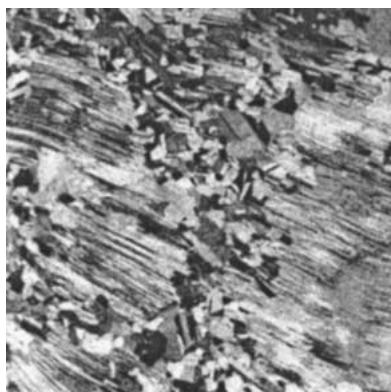
Figure 2 Microstructure for duplex γ-TiAl in the As-received condition.
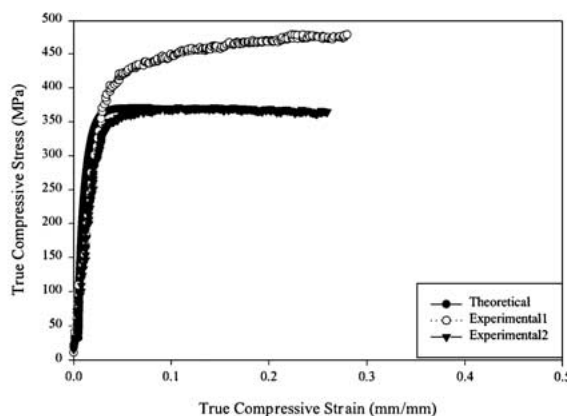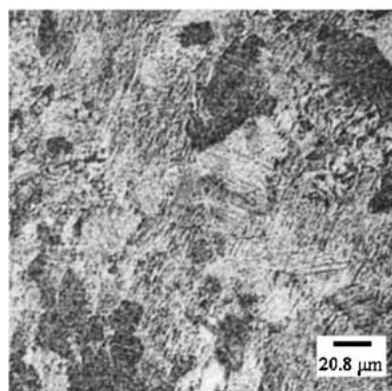
indicates that dynamic recrystallization has occurred. Examining the stress-strain curves, strain hardening was found in both experiment 1 and experiment 2. However, a more drastic increase in stress occurred in the stress-strain curve of experiment 1. In examining the microstructure, the grains in experiment 1 were found to have undergone a more significant amount of dynamic recrystallization. The curves indicate that the higher the percentage of dynamic recrystallization occurring, the higher the strength at this temperature. In the simulation of the curve of experiment 2, the experimental and theoretical values are overlapping. In Fig. 3, the curve has the distinct peak of recrystallization and the slight slant of a curve, which would indicate that the alloy is undergoing softening or recovery. It is assumed that recovery was the governing mechanism during dynamic recrystallization.

In the compression test conducted at 950°C with 0.1/s strain, the lamellar and equiaxed grains have been only slightly recrystallized, as shown in Fig. 4. It appears that the lamellar microstructure has been partially transformed into a duplex microstructure. The equiaxed gamma grains appear to have been partially transformed into a duplex microstructure along the grain boundaries. From the change in the grain size, it can be concluded that dynamic recrystallization has occurred in the grain boundaries of the lamellar grains and equiaxed grains. Since the amount of loading was limited, the controlling mechanism in this test was both strain hardening and recovery. The grains are not as fine as in the 0.001/s strain rate because the recrystallization cycle was not completed. However, the shape of the curve in Fig. 4 indicates that during the elastic deformation process recovery was already occurring and possibly strain hardening also was commencing. However, in the theoretical curve, the assumption was that the high strength was caused by changes in the strain hardening dislocation density. Since the grain sizes were affected as observed in Fig. 4, the movement of dislocations at or across the grain boundaries affected the strength. Also, since the grains consist of both gamma and alpha-two phases, the alpha-two grains adds to the strength initially, with the gamma phase adding to the strength in the higher temperature range as the phases are transformed.

For the compression test conducted at 1000°C with 0.001/s strain rate, significant dynamic recrystallization

Figure 3 Microstructure and stress-strain curves for duplex γ-TiAl (950°C, 0.001/s).
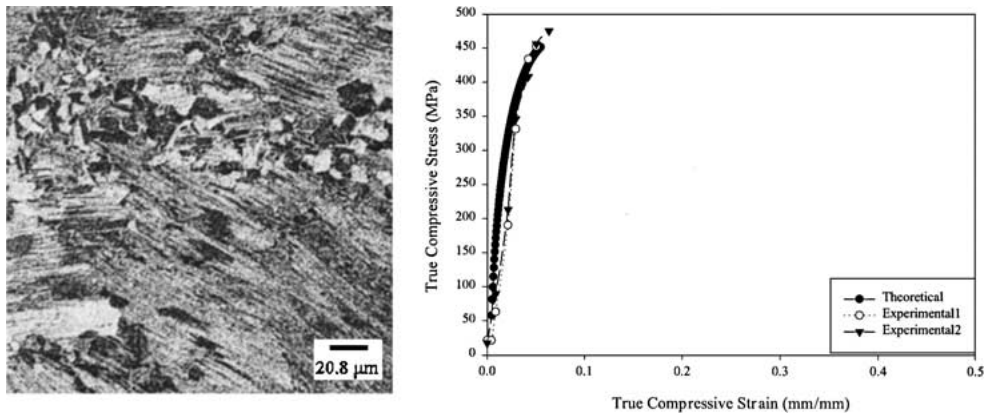
Figure 4 Microstructure and stress-strain curves for duplex γ-TiAl (950°C, 0.1/s).

is observed in the microstructure, Fig. 5, the equiaxed grains have been completely transformed, while the size and spacing of the lamellar grains have been reduced. Regions of precipitate or single-phase concentration that could limit the movement or creation of dislocations are present in the microstructure; the curves from the tests also show a distinct peak at the beginning, followed by slight hardening and then flow softening in a cyclic fashion in Fig. 5. In the numerical simulation, the curve does not have the wavy features due to possible limited dislocation density value or activation energy. However, the theoretical curve does show approximately similar strength. The low activation energy possibly had an effect on the critical dislocation density,

while the initial dislocation density determined the final dislocation density. It is stipulated that the lower values would cause a lower strength. Recrystallization also would occur at a lower value of activation energy. In determining the cause for the higher strength in the experimental curves, the amount of phases present may be used for analysis. Initially, the reduction in the amount of alpha phase would have caused a lower strength, since the dislocations could move more readily across the grain boundaries.

Fig. 6 illustrates the microstructure of the compression test conducted at 1000°C with 0.1/s strain rate. The lamellar grains have been refined with the equiaxed gamma grains being converted to either refined lamellar
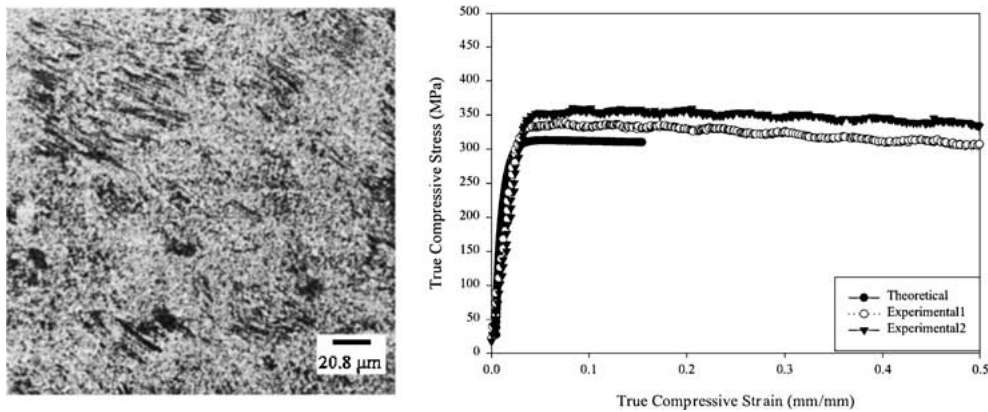
Figure 5 Microstructure and stress-strain curves for duplex γ-TiAl (1000°C, 0.001/s).
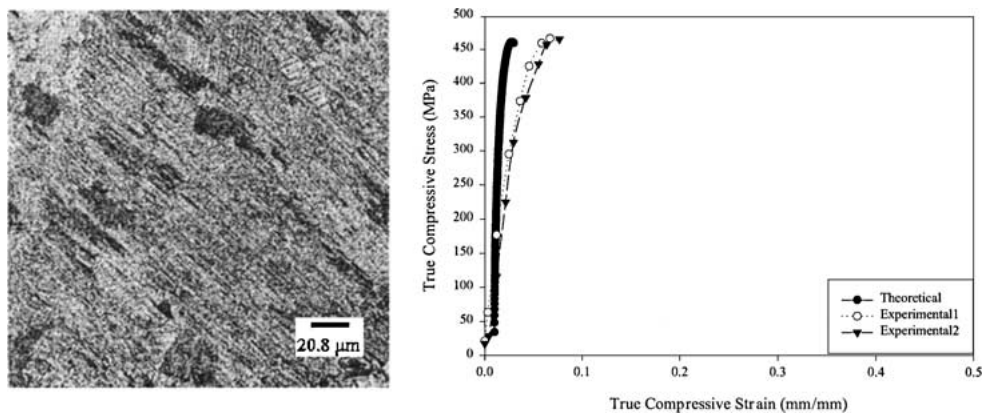
Figure 6 Microstructure and stress-strain curves for duplex γ-TiAl (1000°C, 0.1/s).

or single-phase gamma. The microstructure illustrates that dynamic recrystallization has occurred with the formation of the refined lamellar grains. The completion of the recrystallization process was prevented by the limitation of the load. The changes in the microstructure limit the amount of movement of dislocations. Depending on the type of phases in the concentration regions it will also limit the concentration of dislocations. Since the test was not completed as shown in Fig. 6, the assumption that dynamic recrystallization did occur must be based on the change in the microstructure. The altering mechanism in this test is strain hardening with a small fraction due to recovery. Since the material recrystallized at such a high rate, the dislocations must have been hindered at the grain boundaries, resulting in the rapid increase in strength. At the top of the curve, the strength appears to be leveling off, which could indicate that recovery is commencing. From the recrystallization observed, it can be deduced that the material was undergoing flow softening, since the grains have reached their minimum size. Accounting for the above factors, the stress values for the theoretical curve are high due to the low initial dislocation density and activation energy.

In the compression test conducted at 1100°C at 0.001/s strain rate, the grains had recrystallized and experienced also some grain growth. As shown in Fig. 7, the grains have recrystallized with the grains along the grain boundaries of the lamellar and of the original equiaxed gamma grains beginning to grow. The

microstructure was transformed after recrystallization back into duplex type still containing lamellar grains. The strength is caused by the reduction of the grain size, as the dislocation motion is hindered when the grains contact. As grain growth occurs in the cycle, the strength gradually decreases, Fig. 7. The curves have a distinct peak which indicates that the dislocation density and grain size were being altered; therefore, recrystallization was occurring. In the experimental tests, the curves undergo continuous cycles of recrystallization with the time of recovery increasing with each. Since recovery is being altered during the experimental process, its value is changed during the theoretical simulation. Also, as the dynamic recrystallization is so pronounced, the theoretical values should coincide with experimental values, as the results verify.

In the compression test conducted at 1100°C at 0.1/s strain rate, the microstructure, as seen in Fig. 8, was altered due to the formation of recrystallized grains. Equiaxed grains are reforming along the grain boundaries, but are not as well defined as in the as-received sample. Some among them are much larger in size than in the original sample. The lamellar grains have almost been completely recrystallized and are reforming. Again the duplex structure as in the as-received sample results after recrystallization. In studying the stress-strain curves, the strain rate is apparently lower than the rate necessary to complete the recrystallization cycle; that is the reason why the curve has a cyclic shape (more pronounced in Experiment 2). The curve also
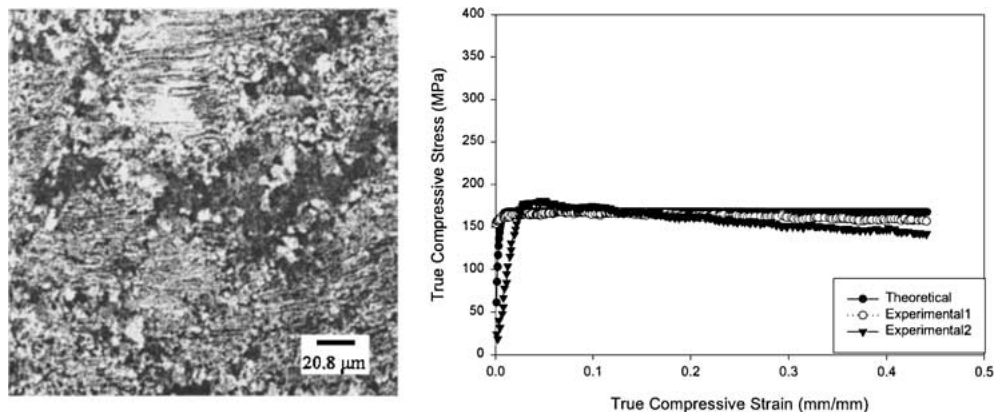
Figure 7 Microstructure and stress-strain curves for duplex γ-TiAl (1100°C, 0.001/s).
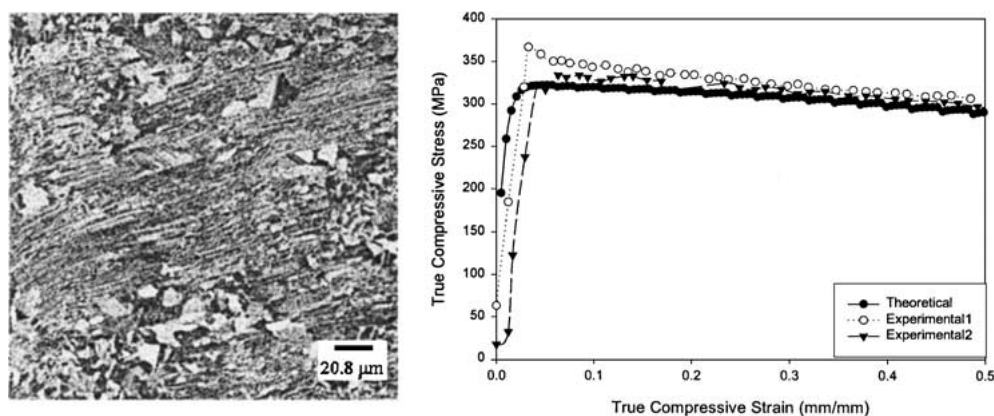
Figure 8 Microstructure and stress-strain curves for duplex γ-TiAl (1100°C, 0.1/s).

indicates that dynamic recrystallization has occurred, with the distinct peak being present, followed by flow softening. Cyclic hardening and recovery are evident from the shape of the curves. The initial transformation of the lamellar and equiaxed gamma grains dominates in the initial strain hardening leading to the flow stress maximum, while reformation of the grains and their growth dominate in the recovery phase. In determining the parameter, both processes had a major effect on the recrystallization of the alloy.

The microstructures thus indicate that dynamic recrystallization does occur at the various selected temperatures and strain rates. The amount of recrystallization in the experiments is significant in some cases depending mostly on the change in temperature and time of compression or strain rate. The strength changes according to the strain rate. The experiments also prove that at high temperature (950°C)/low strain rate dynamic recrystallization is more evident, as shown in Fig. 3 (compared with Figure a corresponding to high strain rate). At still higher temperatures (1000°C) dynamic recrystallization occurs even at higher strain rates probably because of the availability of increased amount of energy for activation of the process, and grain growth after recrystallization becomes evident. It is interesting to note the reformation of the duplex grain structure even after recrystallization at higher temperatures (1100°C).

In the experiments where the final microstructure consisted of recrystallized lamellar grains with equiaxed grains at the boundaries, the numerical simulations of the curves are almost an exact match with the experimental curves. The results are based on the assumption by Hofmann and Blum [16] that a lamellar microstructure can be treated as a single phase. In the experiments where the microstructure consists of recrystallized lamellar grains of either phase or has precipitate concentrations, the results are slightly misaligned. The model simulated the mechanical properties assuming that the proper controlling parameter, i.e. recovery, strain hardening, or recrystallization, was altered and inserting suitable values in the program. Since the alloy consisted of two phases, the amount of dislocations in and properties contributed by one phase dominated the other phase.

In evaluating whether the experimental and theoretical material properties are valid, the microstructure and stress-strain curves must be compared. Under equilibrium conditions, in the phase diagram, the amount of α_2 decreases as the temperature is raised. Since the presence of the α_2 phase causes strengthening, the strength of the material decreases as the temperature increases. Since the assumption that the initial dislocation density did not change was used to simulate the theoretical curve, a constant had to be used in the critical dislocation density equation to ensure that the calculated value would satisfy the following: $\rho_c > \Delta\rho_o$, $\rho_c > \rho_o$, and $\rho_c > \rho_H$. The amount of dislocation due to strain hardening and recovery change with time as illustrated in the Equation 4. In determining the flow curve, fractions of the dislocation density due to work hardening and recovery were used in the program. The fraction of dislocations formed due to hardening and recovery was determined using Equations 5 and 6 (given in Table I).

In Figs 3 and 4, the material has undergone significant strengthening. The initial microstructure has alpha-two along the grain boundary with the grains being majority gamma, which meant that the dislocations were moving across the grains, but were being hindered at the boundaries. Therefore, the flow softening was due to the removal of α_2 phase and dislocations formed during the forging process. As the majority of the phase is transformed to gamma, the material will have a tendency to be ductile. Thus, a high strength material is shown in the stress-strain curve, with flow softening developing after the yield stress is reached. The fractional values of the recovery are affected more than strain hardening.

In Figs 5 and 6, the amount of alpha-two phase has been reduced along with the misalignment of dislocations. The reduction in the alpha-two phase causes the strength to decrease. Since it was assumed that the initial dislocation density was constant, the fractions for the critical dislocation density must be altered to account for the decrease in strength. The strength also decreases with recovery, since an increase in the percent of gamma phase occurs. This increase in gamma allows the dislocations to move more freely as the phase is ductile. However, an increase in strain rate raises the rates of the recrystallization cycle and thus increases the strength. So, to account for the change in dislocation density, fractional values of recovery were lowered to simulate the corresponding curves.

In Figs 7 and 8, the strength further decreases due to the increase in temperature. The strength is still high, as the alpha-two grains are present initially along the grain boundary. However, the effect of the transformation is more evident as the amount of gamma grains and possibly dislocation alignment increase with a concomitant decrease in strength. It seems that the dislocations can move more freely through the material and form at a slower rate. However, this could be elated to the amount of dislocations formed during the recovery process decreases, thus a softening curve is present after the yield stress.

4. Conclusions

1. At high temperature, the change in strain rate has insignificant effect on the microstructure, but alters the strength drastically.

2. The experimental results indicate that the best recrystallization occurs at all high temperatures and strain rates used. However, the most recrystallization occurred at high temperature/low strain rate (resulting in flow softening), with the highest strength at low temperature/high strain rates (due to strain hardening).

3. By using the microstructure and other significant variables, i.e. strain rate, grain size, etc., and an enhanced model integrating the models developed by Sandstrom and Lagneborg, and Pietryzk, the stress-strain curves for the forging process can be derived. The present used integrated model can be utilized to predict the stress-strain curve of a dynamically recrystallized TiAl alloy during the hot forging.

References

1. S. L. SEMIATIN, V. SEETHARAMAN and I. WEISS, *JOM* **49** (1997) 33.
2. P. L. ORSETTI ROSSI and C. M. SELLARS, *Acta Materialia* **45** (1997) 137.
3. C. M. SABINASH, S. M. L. SASTRY and K. L. JERINA, *Materials Science and Engineering* **A192/193** (1995) 837.
4. R. A. MIRSHAMS, Z. X. LI and H. P. MOHAMADIAN, *J. Mater. Sci. Lett.* **16** (1997) 715.
5. R. A. MIRSHAMS, Report to U.S. Army-TACOM, Contract #DAAE07-93-C-R127, June 1997.
6. R. SANDSTROM and R. LAGNEBORG, *Acta Metall.* **23** (1975) 387.
7. R. SANDSTROM and R. LAGNEBORG, *ibid.* **23** (1975) 481.
8. M. PIETRYZK, *Journal De Physique* **IV** (1993) 1163.
9. Metals Handbook, Metallography and Microstructures, Vol. 9, 9th ed. (ASM, 1985) p. 460.
10. A. A. HAMEDA and L. BLAZ, *Scripta Materialia* **37** (1997) 1987.
11. W. ROBERTS and B. AHLBLOM, *Acta Metall.* **26** (1978) 801.
12. V. SEETHARAMAN and S. L. SEMIATIN, *Metallurgical and Materials Transactions A* **27A** (1996) 1987.
13. *Idem.*, *ibid.* **28A** (1997) 2309.
14. S. L. SEMIATIN, V. SEETHARAMAN and V. K. JAIN, *ibid.* **25A** (1994) 2753.
15. V. SEETHARAMAN and S. L. SEMIATIN, *ibid.* **28A** (1997) 947.
16. U. HOFMANN and W. BLUM, *Scripta Metallurgica et Materialia* **32** (1995) 371.
17. K. Y. WANG, R. A. MIRSHAMS and B. Q. LI, in the Conference Proceedings of Advanced Materials Processing, TMS, Honolulu, Hawaii, 1998, p. 2007.
18. M. PIETRYZK, C. ROUCOULES and P. D. HODGSON, in the Conference Proceedings of Simulation of Materials Processing: Theory Methods and Applications, edited by Shen and Dawson (1995) p. 315.
19. M. PIETRYZK, *Metallurgy and Foundry Engineering* **20** (1994) 429.
20. S. ILLENDULA, R. A. MIRSHAMS, W. WANG and B. Q. LI, in Proceedings of the Int. Symposium on Processing of Metals and Advanced Materials, TMS Annual Meeting, San Antonio, 1998, p. 121.
21. U. HOFMANN, R. SEDLACEK and W. BLUM, *Z. Metallkd* **87** (1997) 411.